Tensile behaviour of spring steel wire reinforced EN AW-6082

Matthias Merzkirch, Marius Meissner, Volker Schulze, Kay A. Weidenmann

Angaben zur Veröffentlichung / Publication details:

Merzkirch, Matthias, Marius Meissner, Volker Schulze, and Kay A. Weidenmann. 2015. "Tensile behaviour of spring steel wire reinforced EN AW-6082." *Journal of Composite Materials* 49 (3): 261–74. https://doi.org/10.1177/0021998313517581.

Tensile behaviour of spring steel wire reinforced EN AW-6082

Matthias Merzkirch, Marius Meissner, Volker Schulze and Kay André Weidenmann

Abstract

The reinforcement of composite aluminium extrusions offers a high potential regarding weight reduction and improvement of mechanical properties, which is essential for components in lightweight constructions. The current work gives an overview of the quasi-static properties of spring steel wire reinforced EN AW-6082 with varying reinforcing ratio. The deformation and damage behaviour is investigated in detail for a reinforcing ratio of 11.1 vol.%. It is shown that the relatively ductile behaviour of the spring steel wire leads to multiple necking resulting in higher strains than expected. Current models are expanded and modified for a proper adaptation to the material system.

Keywords

MMC, unidirectionally reinforced, composite extrusion, EN AW-6082, 301SS, multiple necking, Kelly, Courtney, tensile behaviour, ductile reinforcement

Introduction

The composite extrusion process[1] allows a direct embedding of metallic and hybrid wires based on ceramic fibres[2,3] within lightweight metal matrices such as aluminium and magnesium alloys, with the help of modified porthole dies. The current state of the art allows the production of a multitude of different continuous wire reinforced material combinations and profile geometries.[4–7] The maximum reinforcing ratio of the profiles is 13.5 vol.% due to geometric and capacity restrictions of the extrusion press used within the Collaborative Research Center/Transregio 10 focussing on the production and characterization of this novel material class. Possible future applications can be found in the automotive and aerospace sectors.

For this reason it is essential to obtain knowledge of the constituent deformation and damage behaviour as a function of the reinforcing ratio, including reinforcing ratios larger than 13.5 vol.%. The investigations within the current paper therefore deal with the mechanical properties of specimens in which the reinforcing ratio was increased up to 25 vol.% - with a constant reinforcing element diameter of 1 mm - by reducing the specimens' measuring diameter. Beside the influence of a varying reinforcing ratio on the mechanical properties like strength and ductility, the deformation and damage behaviour is investigated in detail for a representative reinforcing ratio of 11.1 vol.%. The aim of the current research is a modification of existing models for an accurate prediction of the mechanical behaviour based on the mechanical properties of the single components.

Iso-strain model

Based on the investigations of Voigt,[8] the tensile behaviour of unidirectionally reinforced composites is discussed in detail in Refs [9,10] using the stress-based rule of mixture (ROM/σ). Altogether four regions of deformation and damage can be described, which are shown in Figure 1.

Within region I pure elastic behaviour is shown where the rule of mixture for the Young's modulus E_I (ROM/E) can be used. The beginning of region II is

Institute for Applied Materials, Karlsruhe Institute of Technology, Karlsruhe, Germany

Corresponding author:
Matthias Merzkirch, Institute for Applied Materials (IAM–WK), Karlsruhe Institute of Technology (KIT), Engelbert-Arnold-Strasse 4, 76128 Karlsruhe, Germany.
Email: Matthias.Merzkirch@kit.edu

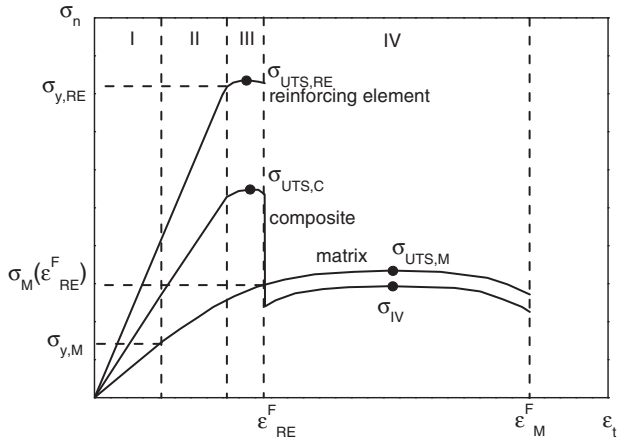

Figure 1. Schematic stress–strain diagram for a composite consisting of a ductile matrix and a ductile reinforcement calculated from the mechanical behaviour of its components.[5]

defined by the onset of plastification of the matrix material at its yield strength $\sigma_{y,M}$. The superposition of the elastic behaviour of the reinforcing element and the elastic-plastic behaviour of the matrix material within region II can be approximated by equation (1):

$$E_{II} = E_{RE} \cdot V_{RE} + \left(\frac{d\sigma_M}{d\varepsilon_M}\right) \cdot V_M \tag{1}$$

The differential coefficient $\left(\frac{d\sigma_M}{d\varepsilon_M}\right)$ describes the slope of the stress–strain curve after onset of plastification and marks the linear approach of the hardening of the unreinforced matrix material. Since the slope during hardening is low in comparison to the Young's modulus of the reinforcing element, equation (1) can be simplified by neglecting the second term. Region III is determined by the plastification of the reinforcing element and does not occur where brittle reinforcing elements are used.[9,10] The ultimate tensile strength of the composite can be calculated as follows:

$$\sigma_{UTS,C} = \sigma_{UTS,RE} \cdot V_{RE} + \sigma_M\left(\varepsilon^F_{RE}\right) \cdot V_M \tag{2}$$

$\sigma_M(\varepsilon^F{}_{RE})$ stands for the stress occurring within the matrix at fracture of the reinforcing element. The fracture of the reinforcing element marks the transition to region IV which represents the elastic–plastic behaviour of the remaining matrix until its final fracture.[10] The ultimate tensile strength of the remaining matrix can be calculated from the volume weighted ultimate tensile strength of the matrix material according to equation (3)[10]:

$$\sigma_{IV} = V_M \cdot \sigma_{UTS,M} \tag{3}$$

It should be noted that these relationships are focussed on the use of ductile reinforcing elements resulting in higher tensile strengths than predicted by the models. This is due to the fact that the reinforced matrix impedes necking, or delays necking to higher stress.[10] The triaxial stress state must also be considered.

Deviation from iso-strain model

Ductile reinforcing elements are able to neck resulting in higher strains of the matrix within the composite than assumed on the basis of the iso-strain model. This leads to a higher strain at fracture of the reinforcing element within the composite compared to the single reinforcing element. Contrary to the iso-strain model the uniform elongation of the composite lies between the uniform elongation of the reinforcing element and that of the matrix (as a function of the reinforcing ratio). This leads to an underestimation of the composite's tensile strength according to equation (2).[9,10]

The investigations carried out in Ref. [11] using optical measurements showed a strain localisation due to which the matrix within the composite bears less strain to fracture than the unreinforced matrix. The expanded iso-strain model of Ref. [11] will be explained in the following paragraphs.

Since the iso-strain model is only valid until fracture of the reinforcing element ε^F_{RE}, a correction of the uniform elongation is made according to equation (4):

$$\varepsilon^{uni}_{t,cor}(\varepsilon_t) = \varepsilon^F_{RE} + \frac{\alpha \cdot L'_0}{L_0 \cdot \left(\varepsilon^{uni}_M - \varepsilon^F_{RE}\right)} \cdot \left(\varepsilon_t - \varepsilon^F_{RE}\right) \quad \text{for } \varepsilon^F_{RE} \le \varepsilon_t \le \varepsilon^{uni}_M \tag{4}$$

as well as the necking strain according to:

$$\varepsilon^{neck}_{t,cor}(\varepsilon_t) = \varepsilon^F_{RE} + \frac{\alpha \cdot L'_0}{L_0} + \frac{\beta \cdot \sqrt{V_M \cdot A_0}}{L_0 \cdot \left(\varepsilon^F_M - \varepsilon^{uni}_M\right)} \cdot \left(\varepsilon_t - \varepsilon^{uni}_M\right) \quad \text{for } \varepsilon^{uni}_M \le \varepsilon_t \le \varepsilon^F_M \tag{5}$$

where L_0 is reduced to the length of the gap L'_0 (close to zero[11]) due to fracture of the reinforcing element. The parameters α and β can be determined according to the following equation for the calculation of the total length to fracture of a specimen.[12]

$$\Delta L_F = \alpha L_0 + \beta\sqrt{A_0} \tag{6}$$

The first term represents elongation without reduction and the second term with reduction (necking) of the cross-sectional area of a specimen.

The presented model was successfully applied to Inconel 601 rope reinforced EN AW-6060-T4 for a reinforcing ratio of 11 vol.% where a good agreement between experiment and model can be shown, see Figure 2.

In Refs [5,11,13], it is shown that for different composite extruded hardenable aluminium alloys (EN AW-2099, EN AW-6056, EN AW-6060-T4, EN AW-6082) with a reinforcing ratio of 11 vol.%, consisting of high-alloyed iron-based reinforcing elements with a diameter of 1 mm, region III showed higher strain until fracture of the reinforcing element compared to the single reinforcing element as expected according to Kelly and Davies.[9] In this regard a modification was made by introduction of the stress at fracture of the reinforcing element within the composite (in order to optimise equation (2)), which leads to a better estimation with the experimentally measured values.[13] The reason for the higher strain was assumed to be multiple necking of the reinforcing element.

The phenomenon of multiple necking has already been confirmed for different material systems with ductile reinforcing elements.[14–17] The most probable explanation can be found in the load transfer (continuous shear interaction) from the matrix to the reinforcing element.[15] Necking of the reinforcing element results in a plastification of the matrix material in the region where necking occurs. This leads to a hardening of the matrix material which in turn causes a necking of the reinforcing element at a different location; this is repeated until the final fracture of the specimen.[15]

The uniform elongation of the composite ε_C^{uni} was quantified under the assumption of ideal interfacial strength and necking of the single components resulting in necking of the composite.[18] The dependence of the reinforcing ratio V_{RE} on the uniform elongation ε_C^{uni} can be expressed as follows:

$$V_{RE} = \frac{1}{1 + \gamma \cdot \frac{(\varepsilon_C^{uni} - \varepsilon_{RE}^{uni})}{(\varepsilon_M^{uni} - \varepsilon_C^{uni})} \cdot (\varepsilon_C^{uni})^{(\varepsilon_{RE}^{uni} - \varepsilon_M^{uni})}} \tag{7}$$

with:

$$\gamma = \frac{\sigma_{UTS,RE}}{\sigma_{UTS,M}} \cdot \frac{(\varepsilon_M^{uni})^{\varepsilon_M^{uni}}}{(\varepsilon_{RE}^{uni})^{\varepsilon_{RE}^{uni}}} \cdot \frac{\exp(\varepsilon_{RE}^{uni})}{\exp(\varepsilon_M^{uni})} \tag{8}$$

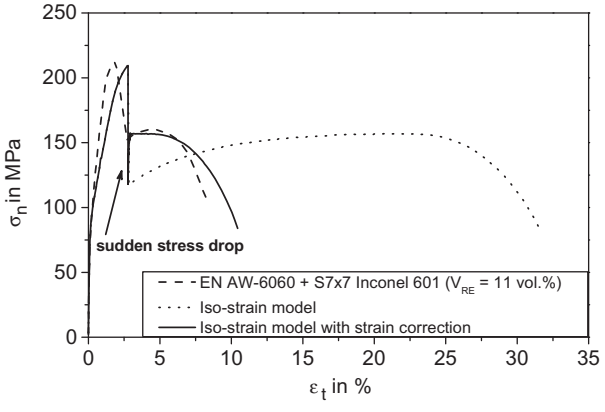

Figure 2. Prediction of the elongation to fracture for an 11 vol.% rope reinforced composite using the iso-strain model and the modification.[11]

Experimental

Materials

The $40 \times 10\,mm^2$ rectangular profiles were manufactured on a 10 MN extrusion press at the Institute of Forming Technology and Lightweight Construction at TU Dortmund University.[1,4] The matrix material is the aluminium alloy EN AW-6082. The measured chemical composition of the matrix material is shown in Table 1 where magnesium and silicon lead to a hardening of the alloy.

The quasi-static properties of the matrix material can be taken from Table 2.

The composition of the reinforcing element with an average diameter of 1 mm made of stainless spring steel 301SS is given in Table 3. The microstructure shows martensite, bainite and also parts of retained austenite.

The quasi-static properties of the reinforcing element can be taken from Table 4. It should be noted that the wire shows plastic deformation.

The composite profiles were made from the same matrix material and additionally reinforced during composite extrusion with four spring steel wires which were embedded in the centre of the $40 \times 10\,mm^2$ profile. Consequently, the reinforcing ratio is about 0.79 vol.%. Prior to the composite extrusion process the matrix material was heated up to a temperature of 500°C, while the ram speed was held constant at 1 mm/s. The press ratio was 42:1. The profile was quenched with ambient air after the extrusion process, followed by natural ageing so that finally the profiles were in heat treatment state T4 (F).

Table 1. Measured chemical composition of the matrix material EN AW-6082 in wt%.

Si	Fe	Cu	Mn	Mg	Cr	Zn	Ti	Al
0.91	0.229	0.031	0.451	0.65	0.044	0.028	0.018	Bal.

Table 2. Quasi-static properties of the matrix material EN AW-6082.

E_M in GPa in %	$R_{p0.2}$ in MPa in %	$\sigma_{UTS,M}$ in MPa in%	ε_M^{uni} in%	ε_{RE}^{F} in%
68 ± 2.9	99 ± 1.3	202 ± 1	$20.7 \pm \Delta\ 1.6$	$28 \pm \Delta\ 0.2$

Table 3. Measured chemical composition of the reinforcing element 301SS in wt%.

C	Si	Mn	P	S	Cr	Ni	Mo	N	Fe
0.074	0.52	0.93	0.034	0.002	18.2	8.3	0.43	0.043	Bal.

Table 4. Quasi-static properties of the reinforcing element 301SS.

E_{RE} in GPa in %	$R_{p0.2}$ in MPa in %	$\sigma_{UTS,RE}$ in MPa in %	ε_{RE}^{uni} in %	ε_{RE}^{F} in %
197 ± 1.4	$1{,}963 \pm 0.5$	$2{,}095 \pm 0.2$	$1.7 \pm \Delta\ 0.02$	$1.8 \pm \Delta\ 0.07$

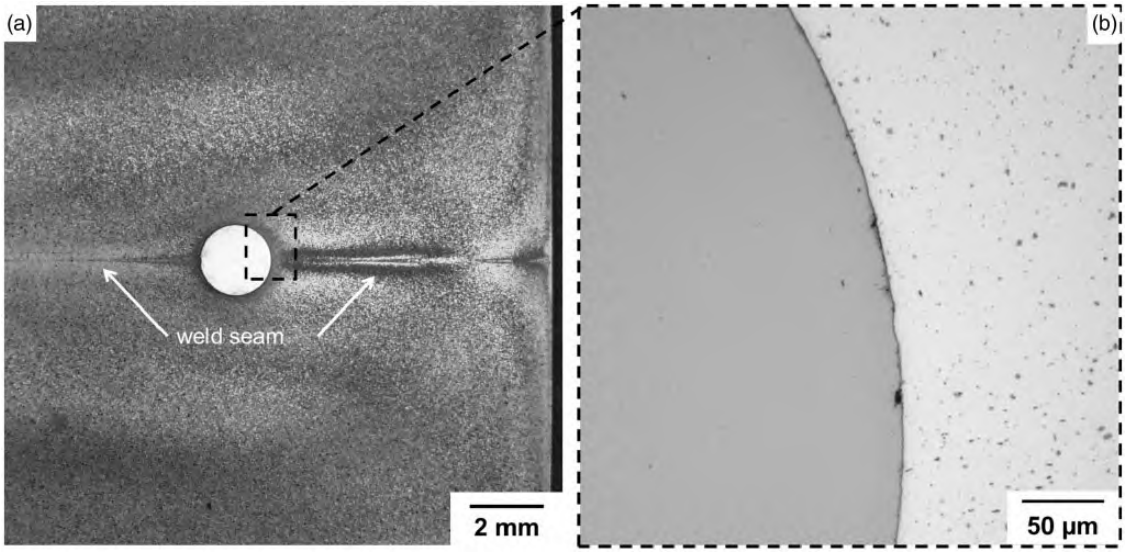

Figure 3. Cross section of a $40 \times 10\,mm^2$ profile: (a) overview etched with 2% hydrofluoric acid, (b) detail of the interface (unetched).

Figure 3(a) shows a detail of an etched (with 2% hydrofluoric acid) cross section of the $40 \times 10\,mm^2$ profile, with the embedded wire and the horizontally placed longitudinal weld seam (arrows) which results from the reconnection of the former split matrix bulk material. Furthermore, a good embedding of the reinforcing element within the matrix can be observed in Figure 3(b). Beside the force closure due to the CTE mismatch, an adhesive bond between matrix and reinforcing element could be observed in Ref. [19].

Specimen geometry

The geometry of the tensile specimens, which were manufactured from the $40 \times 10\ mm^2$ profiles, in order to determine the quasi-static properties with varying reinforcing ratio, is shown in Figure 4.

The reinforcing element with a constant diameter of 1 mm is placed in the centre of the cylindrical specimens (dotted line). The diameter Ø x and the transition radius y were modified depending on the

reinforcing ratio V_{RE}. Table 5 gives an overview of the different specimen diameters with varying reinforcing ratio V_{RE}.

Experimental procedure

The quasi-static tensile tests were performed (with displacement control) on a universal testing machine Zwick with a maximum load of 200 kN. Strain was measured with an integrated Multi-Xtens strain gauge Zwick/Roell. The preload was 100 N.

The displacement rate was set to 1 mm/min resulting in a nominal strain rate of about 8.3×10^{-4} 1/s within the gauge length of 20 mm. The measuring gauge was 15 mm according to a proportional factor length/diameter of five for the unreinforced specimens.

Results

Varying reinforcing ratio

Figure 5 shows representative stress–strain curves illustrating the influence of different reinforcing ratios on the mechanical behaviour.

In general an increasing strength with increasing reinforcing ratio accompanied by a reduction in ductility can be observed. Furthermore a steeper stress slope can be seen within region II. It should be noted that the total strain to fracture of the reinforcing element, characterised by the stress drop, increases with decreasing reinforcing ratio. The total strain at a reinforcing ratio of 25 vol.% is about three times that of the single reinforcing element (compare Table 4).

This behaviour becomes apparent in the plateau region (region III) in which length and slope increases with decreasing reinforcing ratio. Since the proportionality between initial measuring length and varying specimen diameter changes, no conclusion can be drawn about the necking behaviour as a function of the reinforcing ratio V_{RE}.

In the following paragraphs, the average values are shown and described individually. Figure 6 shows the evolution of the slope for the region I (E_I) and II (E_{II}) of the experimental and of the calculated values. Starting with a Young's modulus of about 68 GPa of the matrix and of 197 GPa of the reinforcing element (compare Table 2 and Table 4) the calculated values of the composite stiffness show a good agreement with the experiment despite the measuring uncertainties.

Figure 6(b) visualises the comparison of the experimental data and the rules of mixture expressed in equation (1) and under negligence of the term of the matrix material. E_{II} for $V_{RE} = 0$ vol.% represents the linear strain hardening of the matrix between $\varepsilon_{pl} = 0.2\%$ to $\varepsilon_t = 2\%$. For small reinforcing ratios up to about $V_{RE} = 8$ vol.%, a good agreement can be stated for both rules of mixture whereas the simplified rule of

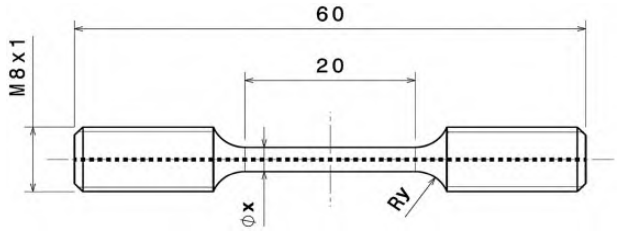

Figure 4. Specimen geometry with varying measuring diameter Ø x with dimensions in mm.

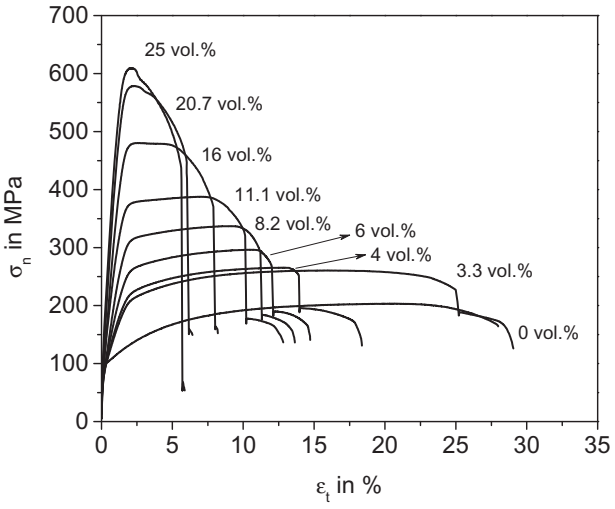

Figure 5. Representative stress–strain curves for different reinforcing ratios.

Table 5. Variation of the specimen diameter Ø with corresponding reinforcing ratio V_{RE}.

	Unreinforced	Reinforced							
specimen-Ø x in mm	3.0	5.5	5.0	4.1	3.5	3.0	2.5	2.2	2.0
V_{RE} in vol.%	0.0	3.3	4.0	6.0	8.2	11.1	16.0	20.7	25.0

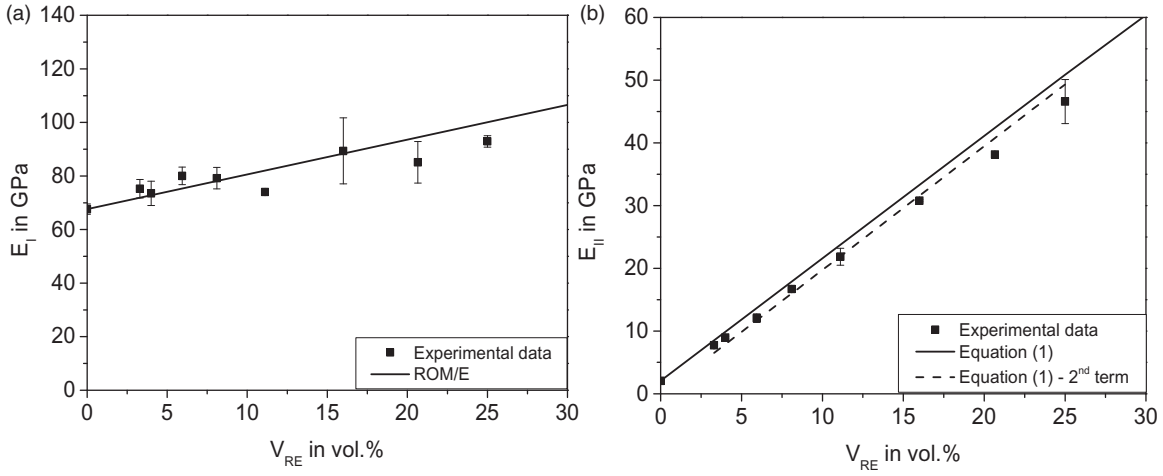

Figure 6. Young's moduli E_I (a) and E_{II} (b) plotted against the reinforcing ratio V_{RE} in comparison to the rules of mixture.

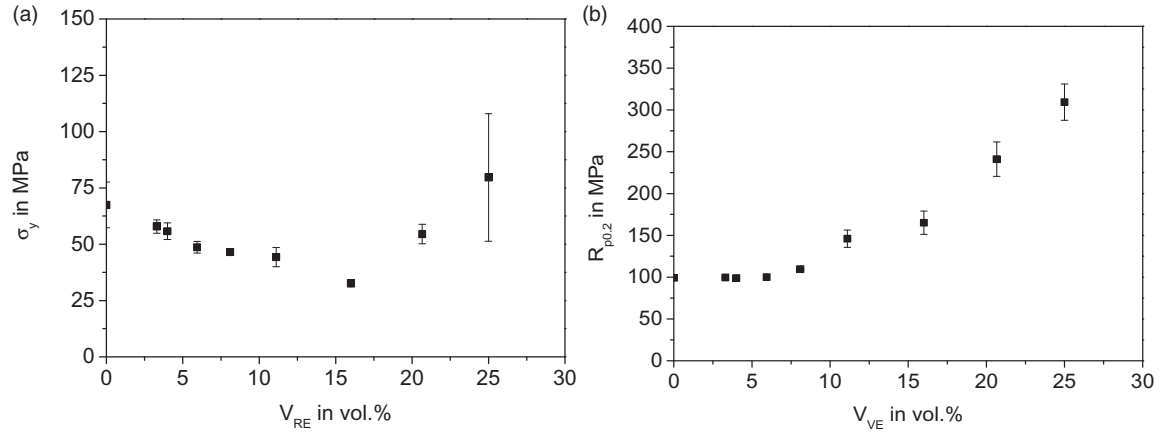

Figure 7. Yield strength σ_y (a) and offset yield strength $R_{p0.2}$ (b) plotted against the reinforcing ratio V_{RE}.

mixture shows a smaller overestimation for higher reinforcing ratios than equation (1).

The comparison of the stiffness within region II shows smaller fluctuations, which can be attributed to the larger analysis area.

Similar to the increasing measuring uncertainties of the Young's modulus E_I, Figure 7(a) shows the evolution of the yield strength σ_y as a function of the reinforcing ratio V_{RE}.

The yield strength was determined by a recognizable deflection of the Young's modulus' linear slope (about 1% deviation from linearity, according to the procedure described in Refs [20,21]). Up to $V_{RE} = 16$ vol.%, a decrease in the yield strength can be observed until an increase can be seen. The high fluctuations of about 35% at a reinforcing ratio of 25 vol.% can be attributed to measuring uncertainties.

Figure 7(b) shows the evolution of the offset yield strength $R_{p0.2}$ plotted against the reinforcing ratio. Up to $V_{RE} = 6$ vol.% almost constant values of about 100 MPa were measured. Starting at a reinforcing ratio of 11.1 vol.% an increase of about 47% can be observed in comparison to the unreinforced material. At a reinforcing ratio of $V_{RE} = 25$ vol.% an increase in the offset yield strength of about 200% in comparison to the unreinforced material can be observed.

Figure 8 illustrates the correlation of the ultimate tensile strength of the composite σ_{UTS} as a function of the reinforcing ratio where a steady linear increase is observable.

The prediction (equation (2)) shows a clear underestimation of the composites' ultimate tensile strength for small reinforcing ratios. With increasing reinforcing ratio the difference between experimental and calculated data decreases, which can be attributed to the decreasing influence of the stress acting within the matrix material at fracture of the reinforcing element.

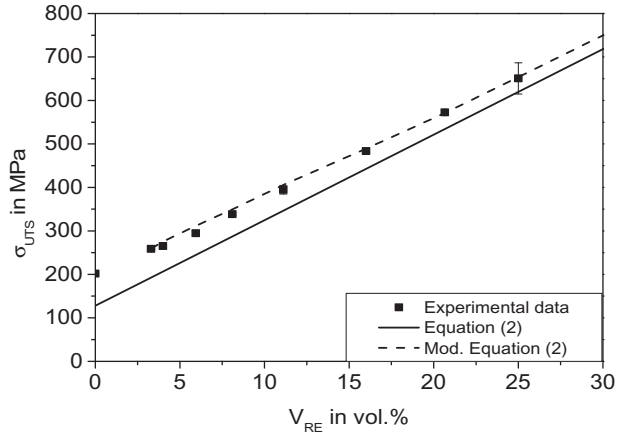

Figure 8. Ultimate tensile strength σ_{UTS} plotted against the reinforcing ratio V_{RE} in comparison to the rules of mixture.

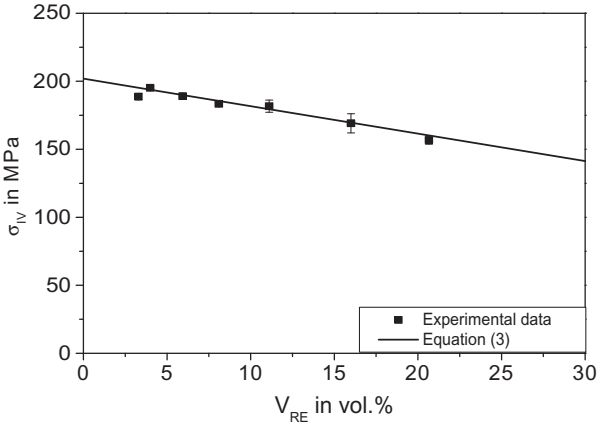

Figure 10. Ultimate tensile strength of the remaining matrix σ_{IV} as a function of the reinforcing ratio V_{RE} in comparison to equation (3).

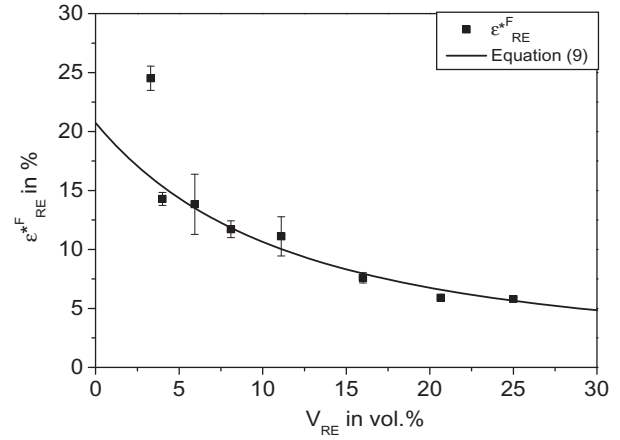

Figure 9. Measured total strain at fracture of the reinforcing element within the composite ε^{*F}_{RE} plotted against the reinforcing ratio V_{RE} and calculated using equation (9).

The comparison of the modified rule of mixture according to Hammers et al.,[13] which includes the stress within the unreinforced material at the strain at fracture of the reinforcing element within the composite, shows a good agreement with the experimental data.

One disadvantage of this procedure for the estimation of the ultimate tensile strength of the composite is the lack of knowledge of the total strain at fracture of the reinforcing element within the composite ε^{*F}_{RE}. As can be seen from Figure 9, this strain is clearly influenced by the reinforcing ratio.

It was determined that the reinforcing element within the composite bears much higher strain to fracture than expected from the single component (compare Table 4).

Figure 10 depicts the comparison of the measured and calculated ultimate tensile strength of the remaining matrix σ_{IV} according to equation (3) where a good agreement can be observed. The reinforcing ratio of $V_{RE} = 25$ vol.% is not displayed since no comparable behaviour was determined for region IV among the three specimens.

Characterization of the composite with a reinforcing ratio of 11.1 vol.%

Since a pronounced strengthening effect can be seen using the offset yield strength from 11.1 vol.% onwards (compare Figure 7(b)), a detailed view of the damage and deformation behaviour (since the factor of proportionality of unreinforced and 11.1 vol.% reinforced specimens is equal) will be presented.

Figure 11 shows the deformation and damage behaviour of an 11.1 vol.% reinforced specimen in heat treatment state T4 (F) with the marked regions I–IV.

The stress-strain curve of the composite shows, after a steep increase of the stress up to about 375 MPa (see point a), a flat region up to $\varepsilon_t \approx 7.5\%$ followed by a steady stress reduction (see point b) until the fracture of the reinforcing element, which can be identified by the sudden stress drop at a total strain of about $\varepsilon_t \approx 10\%$ (see point c). Afterwards a small increase in stress can be observed as well as the deformation of the matrix material until the complete fracture of the specimen at a total strain of about $\varepsilon_t \approx 13\%$.

Metallographic and fractographic investigations

In order to carry out a phenomenological investigation of the damage behaviour under tensile loading, tests

were interrupted at certain total strains ε_t (7%, 9%, 10.5%, see Figure 11) and longitudinal sections of 11.1 vol.% reinforced specimens were prepared.

In Figure 12, multiple necking areas can be seen along the reinforcing element. Furthermore, a deflection of the specimen can be observed due to the slightly eccentric placing of reinforcing element resulting in residual stresses after deformation and unloading.

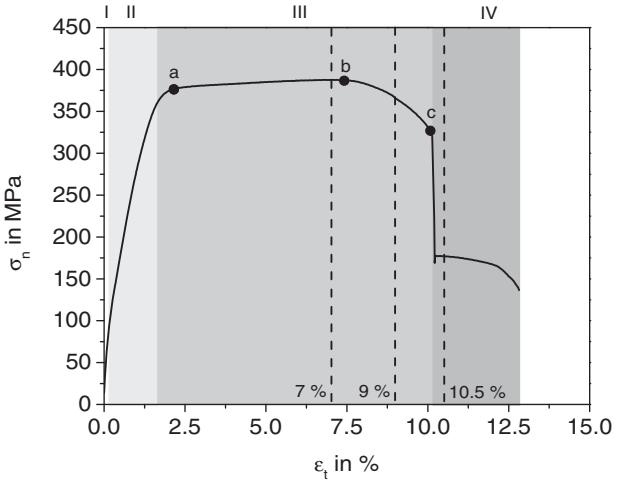

Figure 11. Representative stress–strain curve of an 11.1 vol.% reinforced specimen with indications of the different deformation and damage regions I–IV and the strains for the interrupted tests.

Figure 13 shows a longitudinal section of a specimen which was loaded up to a total strain of $\varepsilon_t = 9\%$, immediately after the decrease in stress prior to fracture of the reinforcing element. The deflection of the specimen is less pronounced than in Figure 12.

It is noticeable in particular that an advanced necking of the reinforcing element additionally leads to a debonding of the interface (Figure 13, left side). A deformation of the matrix material in radial direction to the centre of the specimen can also be observed. Furthermore, the multiple necking of the reinforcing element along the axis can be seen. There is also a necking of the specimen's outer surface within the matrix material (right and left side). An explicit plastic deformation within the matrix material at the most pronounced necking of the reinforcing element can be observed.

Figure 14 shows a longitudinal section immediately after fracture of the reinforcing element. The multiple necking of the reinforcing element as well as the debonding of the reinforcing element from the matrix can be observed.

Due to the fracture of the reinforcing element followed by a decrease of the residual stresses no deflection of the specimen can be seen anymore.

Furthermore an axial crack can be seen within the reinforcing element, starting from the fracture surfaces. The distance between the two fracture surfaces is about 270 µm. The delamination length at the fracture area of the reinforcing element is about 1 mm.

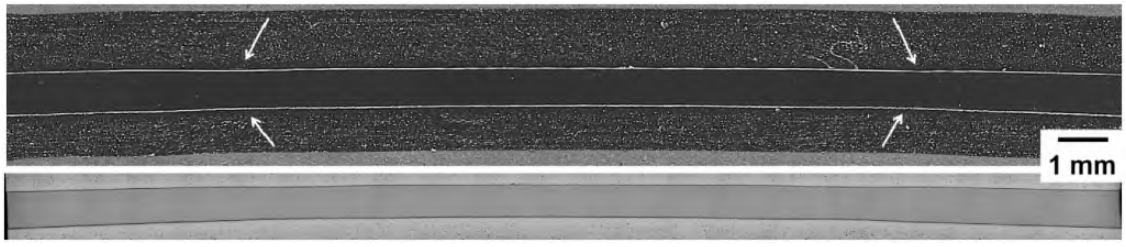

Figure 12. Longitudinal section of an 11.1 vol.% reinforced specimen at $\varepsilon_t = 7\%$ (top: overview, bottom: view along interface).

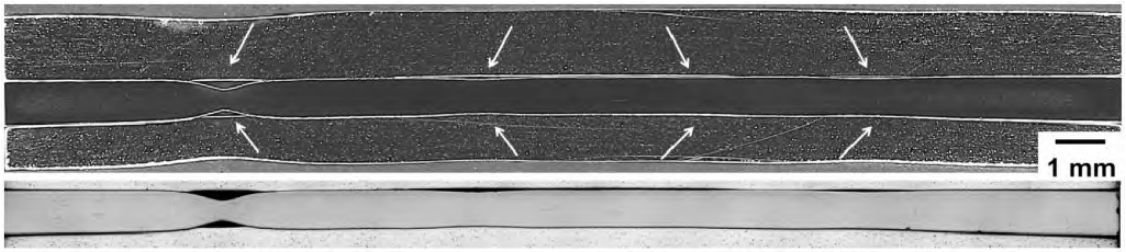

Figure 13. Longitudinal section of an 11.1 vol.% reinforced specimen at $\varepsilon_t = 9\%$ (top: overview, bottom: view along interface).

Figure 15 shows the fracture surfaces with details of the reinforcing element (c) and the matrix material (d). It can be seen that the reinforcing element is in a slightly eccentric position. Due to the necking of the reinforcing element and the delamination occurring in this region, a gap can be seen between the two components (b). The split weld seam at the interface is indicated by arrows, Figure 15(b)).

Modelling

In Ref. [11], an advanced description of the tensile behaviour of unidirectionally reinforced composites after fracture of the reinforcing element in comparison to Ref. [10] is presented. It is assumed that the remaining matrix deforms similarly to the unreinforced matrix material according to the iso-strain model. The parameters α and β needed in equations (4) and (5) were determined using equations (6) to $\alpha = 0.2$ and $\beta = 0.4$, see Ref. [11]. The reduced measuring length L'_0 was determined to 1 mm according to the length of the gap in Figure 14.

The modification of the strain calculation within region IV according to Weidenmann et al.[11] leads to a reduction of the predicted strains. Figure 16 illustrates the comparison between the experimentally

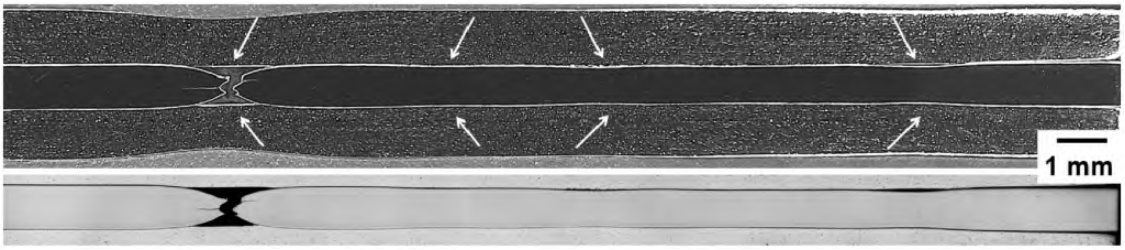

Figure 14. Longitudinal section of an 11.1 vol.% reinforced specimen at $\varepsilon_t = 10.5\%$ (top: overview, bottom: view along interface).

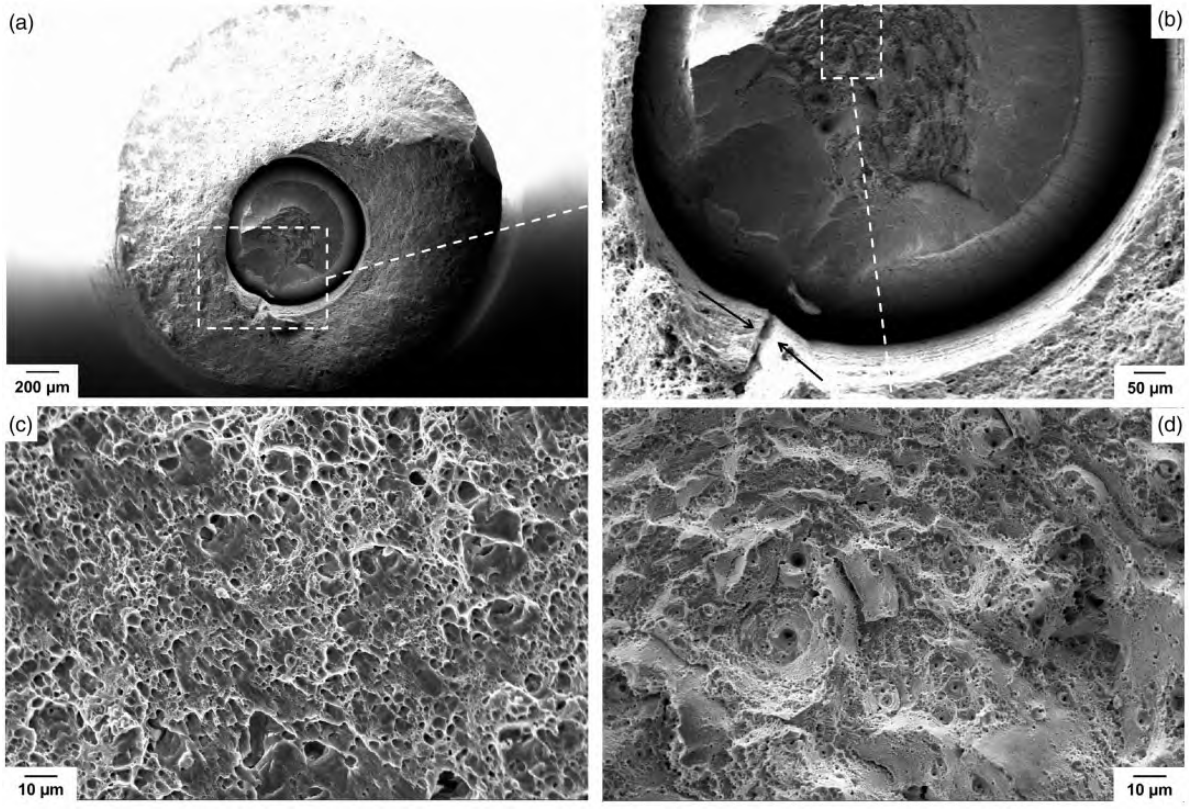

Figure 15. SEM-pictures of the fracture surfaces of an 11.1 vol.% reinforced specimen: (a) overview, (b) interface, (c) fracture surface of the reinforcing element, (d) fracture surface of the matrix.

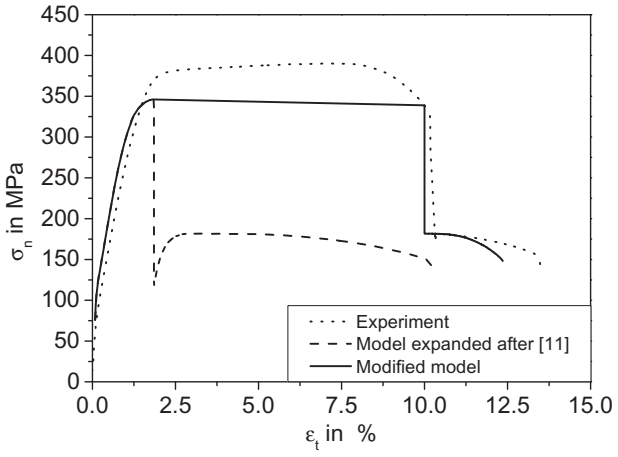

Figure 16. Comparison between measured stress–strain curve, expanded model behaviour according to Weidenmann et al.[11] the modified model behaviour of a 11.1 vol.% reinforced specimen.

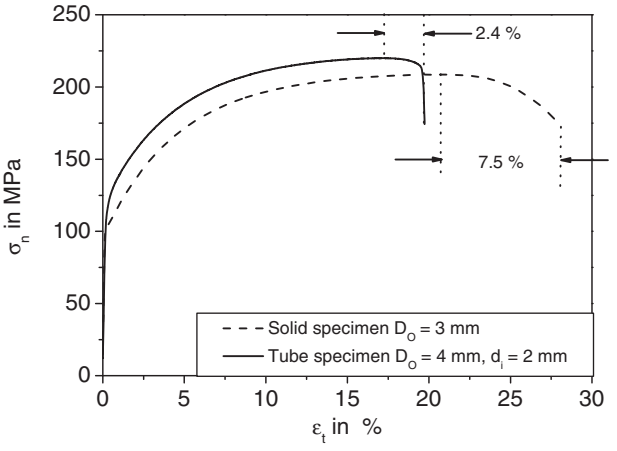

Figure 17. Representative stress–strain curves of solid specimen and a tube specimen.

determined stress-strain curve of an 11.1 vol.% reinforced specimen and the modified model according to Weidenmann et al.[11]

First, a good agreement between experiment and model can be observed for region I whereas region II shows a slight overestimation compared to the experiment. The transition from region II to region III can be precisely predicted concerning the occurring strains whereas the predicted stress level prior to the assumed fracture of the reinforcing element lies about 30 MPa beneath the experimentally determined stress. The occurring stress within the remaining matrix after fracture of the reinforcing element is underestimated by the model. It is noticeable that the model leads to a conservative estimation of the deformation and damage behaviour within region III as well as an optimistic estimation of the matrix deformation within region IV.

The uniform deformation of the composite ε_C^{uni} as a function of the reinforcing ratio V_{RE} was quantified by Ref. [18] (compare equations (7) and (8)). Since the necking behaviour or the necking strain of the composite is strongly dependent on the reinforcing ratio, equation (9) includes a modification of equation (7) concerning the total strain to fracture of the reinforcing element within the composite ε_{RE}^{*F}.

$$V_{RE} = \frac{1}{1 + \gamma \cdot \frac{(\varepsilon_{RE}^{*F} - \varepsilon_{RE}^{uni})}{(\varepsilon_M^{uni} - \varepsilon_{RE}^{*F})} \cdot (\varepsilon_{RE}^{*F})^{\varepsilon_{RE}^{uni} - \varepsilon_M^{uni})}} \tag{9}$$

Figure 9 illustrates the comparison between the experiment and the calculated total strain at fracture of the reinforcing element within the composite ε_{RE}^{*F} as a function of the reinforcing ratio V_{RE}. The needed uniform elongation of the two components (for $V_{RE} = 0$ vol.-% and $V_{RE} = 100$ vol.-%) can be taken from Table 2 and Table 4. A very good agreement with the experimentally determined data can be observed, except for a reinforcing ratio of 3.3 vol.%.

As the investigations have shown, the composite and the reinforcing element neck within region III at a strain of about $\varepsilon_t \approx 7\%$ (compare Figure 12). The necking is a result of the multiple necking of the reinforcing element as well as of the matrix material at the most pronounced necking of the reinforcing element. Therefore equation (4) for the calculation of the uniform elongation after fracture of the reinforcing element will be neglected for the further investigations.

Since the necking initiation after fracture of the reinforcing element occurs from the former interface as well as from the specimen's outer surface, the necking behaviour of the matrix material will now be discussed in detail. For this purpose, unreinforced tube specimens (due to production reasons) with an inner diameter d_i of 2 mm and an outer diameter D_O of 4 mm were manufactured, which is comparable to 11.1 vol.% reinforced specimens with a wall thickness of 1 mm. The initial measuring length was 18.4 mm according to similar length/cross section relation of an initial measuring length of 15 mm, an outer diameter of 3 mm and an inner diameter of 1 mm of 11.1 vol.% reinforced specimens. Figure 17 shows the stress–strain curves of solid specimens and tube specimens. The higher strength of the tube specimen will be neglected.

Since tube specimens neck from the inside as well as from the outside, the necking strain of the tube specimen is about a factor 0.32 (2.4%/7.6%) compared to the solid specimen.

The following equation can be given under consideration of the factor 0.32 within the second term of equation (4):

$$\varepsilon_{\mathrm{t,cor}}^{\mathrm{neck}}(\varepsilon_{\mathrm{t}}) = \varepsilon_{\mathrm{RE}}^{*\mathrm{F}} + 0.32 \cdot \frac{\beta \cdot \sqrt{\mathrm{V_M} \cdot \mathrm{A_0}}}{\mathrm{L_0} \cdot \left(\varepsilon_{\mathrm{M}}^{\mathrm{F}} - \varepsilon_{\mathrm{M}}^{\mathrm{uni}}\right)} \cdot \left(\varepsilon_{\mathrm{t}} - \varepsilon_{\mathrm{M}}^{\mathrm{uni}}\right) \quad \text{for } \varepsilon_{\mathrm{M}}^{\mathrm{uni}} \le \varepsilon_{\mathrm{t}} \le \varepsilon_{\mathrm{M}}^{\mathrm{F}} \tag{10}$$

The comparison of the modified model behaviour for regions III and IV with the experimentally determined stress–strain curve is shown in Figure 16.

A relatively good agreement can be observed between the modified model and the experimentally determined stress–strain curve with respect to the strain. The deviation results from the changed specimen geometry as well as from the proportionality between the initial measuring length and the initial cross section.

First it can be attested that the composite strain, which occurs at the beginning of the plateau region ($\sigma_{\mathrm{C}} \approx 382\,\mathrm{MPa}$, $\varepsilon_{\mathrm{t}} \approx 1.9\%$), is underestimated by about 35 MPa. In order to calculate the needed stress within the matrix σ_{M} for the measured composite stress in the plateau region the following transposed equation (2) gives:

$$\sigma_{\mathrm{M}} = \frac{(382\mathrm{MPa} - 2095\mathrm{MPa} \cdot 11.1\mathrm{vol.\%})}{(1 - 11.1\mathrm{vol.\%})} = 168\,\mathrm{MPa} \tag{11}$$

This stress is measured within the unreinforced matrix material at a total strain of about $\varepsilon_{\mathrm{t}} \approx 5.1\%$. The stress measured at a strain of $\varepsilon_{\mathrm{t}} \approx 1.9\%$ according to the model is about 131 MPa. Consequently, the assumed condition of iso-strain according to Ref. [8] loses its validity even prior to necking of the components.

According to Kelly and Davies,[9] a higher composite strength can be measured by using ductile reinforcing elements as predicted by the model. The reinforced matrix leads to a suppression of the early necking of the reinforcing element, or not until a higher stress is reached.

The deformation of the matrix after fracture of the reinforcing element is slightly underestimated in terms of the total strain whereas the strength of the remaining matrix shows a good agreement with the experiment. It can be observed that the model leads to a good estimation of the composite behaviour.

Discussion

It could be shown that the rules of mixture for the determination of the stiffness in regions I and II according to Kelly and Davies[9] are in good agreement with the experimental data (compare Figure 6). It should be noted that a better agreement for the stiffness in region II can be observed under consideration of the strain hardening of the matrix material. Similarly, the prognoses for the determination of the composite strength as well as the strength of the remaining matrix show a good agreement with the measured values. According to Kelly and Davies,[9] the critical reinforcing ratio, at which the reinforcement leads to an increase of the ultimate tensile strength, is about

$$\mathrm{V_{RE,crit}} = \frac{\sigma_{\mathrm{UTS,M}} - \sigma_{\mathrm{M}}(\varepsilon_{\mathrm{RE}}^{\mathrm{F}})}{\sigma_{\mathrm{UTS,RE}} + \sigma_{\mathrm{UTS,M}} - \sigma_{\mathrm{M}}(\varepsilon_{\mathrm{RE}}^{\mathrm{F}})} = 3.7\mathrm{vol.} - \% \tag{12}$$

The steady increase of the ultimate tensile composite strength, shown in Figure 8, which is in a good agreement with the model behaviour, can be attributed to the ductility of the reinforcing element.[9,10] The use of the modified rule of mixture for the determination of the ultimate composite strength under consideration of the matrix stress at fracture of the reinforcing element within the composite[13] leads to an improvement compared to the behaviour predicted by Kelly and Davies.[9] The disadvantage is the necessity of the knowledge of this strain which is significantly affected by the reinforcing ratio (see Figure 9).

Furthermore, Figure 10 shows a good agreement between the estimation of the strength of the remaining matrix and the experimental data.

The decrease of the yield strength with increasing reinforcing ratio (compare Figure 7(a)) can probably be attributed to the residual stresses due to the production process. Additionally, turning of specimens for different reinforcing ratios results in a decrease of the matrix portion which leads to higher residual stresses with increasing reinforcing ratio.

The decrease of the yield strength with increasing reinforcing ratio was already noted in Refs [20] and [21] for particle reinforced aluminium matrix composites. The investigations based on simulations have shown that during pure elastic loading plasticity already occurs in the vicinity of the particles. This leads to the assumption that the effect shown in Figure 7(a) can be explained by the increasing interface-circumference-to-matrix-volume ratio. This would enable plastification of the matrix material around the reinforcing element. The increase in the yield strength from 20 vol.% onwards can probably be attributed to the more significant influence of the pre-plastification by an additional bending component which results from the eccentric wire position.

Furthermore, the increase in the offset yield strength $\mathrm{R_{p0.2}}$ as well as the evolution of the stiffness in region II (Figure 6 (right)) with increasing reinforcing ratio shows an increasing hardening behaviour which could

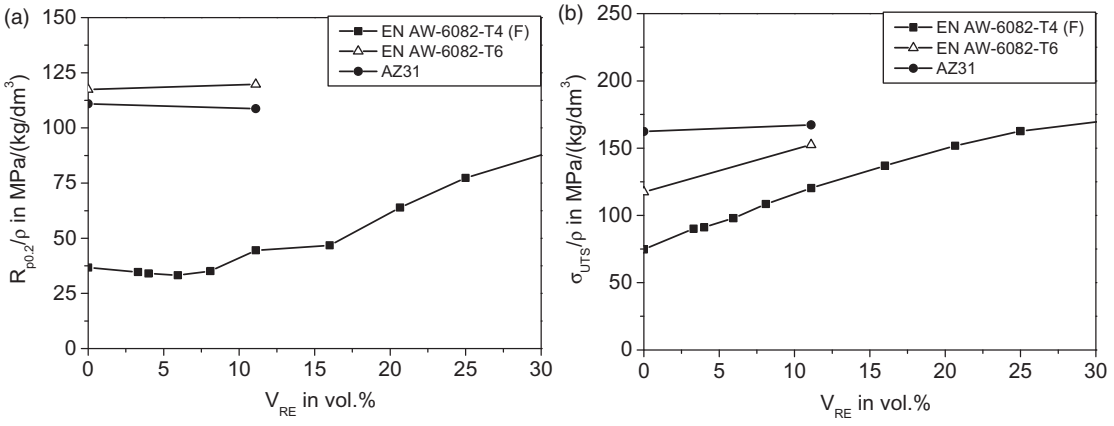

Figure 18. Evolution of the specific offset yield strength $R_{p0.2}/\rho$ (a) and the specific ultimate tensile strength σ_{UTS}/ρ (b) plotted against the reinforcing ratio V_{RE} of EN AW-6082 in heat treatment states T4 (F) and T6 and of AZ31.[25]

also be shown in Ref. [20] for particle reinforced aluminium matrix composites.

It should be added that the procedure, described in Refs [22,23], for the determination of the residual stresses within the composite from the stress–strain curves of the single components could not be applied.

The reason why the modified iso-strain model deduced by Weidenmann et al.[11] could not be adapted to the investigated material system is the high strain of the composite until fracture of the reinforcing element due to its multiple necking.

Comparable observations were made for aluminium-steel composites by Hammers et al.[13] and Shorshorov et al.[17] as well as for tungsten reinforced copper.[14] Similar to the investigations carried out in Ref. [15] on tungsten reinforced brass, Figure 9 shows a decrease of the strain until fracture of the reinforcing element with increasing reinforcing ratio. In Ref. [16], an exponential decrease of the strain at reinforcing element fracture with increasing reinforcing ratio was stated. The model deduced by Mileiko[18] could successfully be adapted to the measured strain to fracture of the reinforcing element within the composite. The characteristic of the necking is influenced by the number of necking areas or the distance of necking areas, as well as the degree of necking (radial deformation necking strain).[14] A quantification of the multiple necking could be made via micro hardness tests in the future.

Within lightweight design beside the specific stiffness E/ρ the specific offset yield strength $R_{p0.2}/\rho$ is also of great importance.[24] Since the spring steel reinforcing element has a similar specific stiffness to the EN AW-6082 matrix (E/ρ (EN AW-6082) $\approx$ 25.9, E/ρ (301SS) $\approx$ 25, E/ρ (AZ31) $\approx$ 23.6), the variation of the reinforcing ratio does not lead to a significant change. Figure 18(a) shows the relation between the specific offset yield strength $R_{p0.2}/\rho$ and the reinforcing ratio V_{RE} of EN AW-6082 in heat treatment states T4 (F) and T6 (solution annealed, quenched with water, artificially aged) and the magnesium alloy AZ31 for an additional optimization in density. For EN AW-6082-T4 (F) a slight decrease of the offset yield strength $R_{p0.2}/\rho$ can be seen up to about $V_{VE} = 6$ vol.%, which can be attributed to the constant offset yield strength $R_{p0.2}$ (compare Figure 7 (right)) and the increasing density (which can also be seen for AZ31 + 11.1 vol.%). A significant increase in the specific offset yield strength $R_{p0.2}/\rho$ can be observed, starting from a reinforcing ratio of 11.1 vol.%.

It should be noted that specimens in heat treatment state T4 (F) with a reinforcing ratio of 25 vol.% show a 30% smaller specific offset yield strength in comparison to unreinforced specimens in heat treatment state T6. The lightweight potential of the T4 (F) composite with a reinforcing ratio of 25 vol.% is exceeded by a heat treatment state T6 and the magnesium alloy AZ31.

The evolution of the specific ultimate tensile strength σ_{UTS}/ρ is shown in Figure 18 (right). It can be concluded that specimens in heat treatment state T4 (F) with a reinforcing ratio of 25 vol.% show a specific ultimate tensile strength comparable to that of unreinforced specimens in heat treatment state T6 and AZ31 + 11.1 vol.%.

Conclusions

The current investigations involved the quasi-static characterization of spring steel wire (with a constant diameter of 1 mm) reinforced EN AW-6082 in heat treatment state T4 (F) for varying the reinforcing ratio up to $V_{RE} = 25$ vol.%. The analyses were accompanied by metallographic investigations and an adaption to current deformation and damage models.

The following conclusion can be drawn:

- Within the composite the reinforcing element shows higher strain to fracture than the single reinforcing element. With decreasing reinforcing ratio, the strain to fracture of the embedded reinforcing element increases significantly due to multiple necking.
- Current models for prognosis of the tensile behaviour based on iso-strain could be modified under consideration of the multiple necking of the reinforcing element as a function of the reinforcing ratio.
- The necking behaviour of the remaining matrix material could also be described for a proper adaption to current damage models.
- In terms of the lightweight potential, EN AW-6082 in heat treatment state T6 or AZ31 with an additional use of reinforcing elements like aluminium oxide fibre reinforced aluminium wire[2,3] would be desirable in order to improve the specific strength and stiffness in comparison to spring steel wire reinforced EN AW-6082 in heat treatment state T4 (F).

Funding

This paper is based on investigations of the subproject A3 – "Material systems for reinforced and functional extruded profiles" – of the Collaborative Research Center/Transregio 10 which is kindly supported by the German Research Foundation (DFG).

Conflict of interest

None declared.

References

1. Kleiner M, Schomäcker M, Schikorra M, et al. Manufacture of extruded and continuously reinforced aluminum profiles for ultra-lightweight constructions. *Materwiss Werksttech* 2004; 35: 431–439.
2. Weidenmann KA, Schomäcker M, Kerscher E, et al. Composite extrusion of aluminium matrix specimens reinforced with continuous ceramic fibres. *Light Metal Age* 2005; 63: 6–10.
3. Merzkirch M, Weidenmann KA, Kerscher E, et al. Mechanical properties of hybrid composite extrusions of an aluminum-alumina wire reinforced aluminum alloy. In: *Proceedings of Materials Science & Technology Conference and Exhibition (MS&T'08)*, Pittsburgh 2008, pp.2552–2562.
4. Pietzka D, Khalifa NB, Gerke S, et al. Composite extrusion of thin aluminum profiles with high reinforcing volume. *Key Eng Mater* 2013; 554–557: 801–808.
5. Weidenmann KA, Kerscher E, Schulze V, et al. Mechanical properties of compound-extruded aluminium-matrix profiles under quasi-static loading conditions. *Adv Mater Res* 2006; 10: 23–34.
6. Hammers T, Kerscher E, Weidenmann KA, et al. Mechanical properties of compound extruded unidirectional reinforced aluminum alloys under quasi-static loading. In: Hirsch J, Skrotzki B, Gottstein G (eds) *Aluminium alloys, vol. 2, their physical and mechanical properties*. WILEY-VCH, 2008, pp.2245–2250.
7. Merzkirch M, Reeb A, Weidenmann KA, et al. Acoustic response of reinforced lightweight metal matrix composites during tensile and cyclic loading. *J Acoust Emission* 2011; 29: 317–328.
8. Voigt W. Theoretische Studien über die Elasticitätsverhältnisse der Krystalle. 1887; K1 34: pp.3–51.
9. Kelly A and Davies J. The principles of the fibre reinforcement of metal. *Metallurgic Rev* 1965; 10: 1–78.
10. Courtney Th. *Mechanical behavior of materials*. 2nd ed. McGraw-Hill, 2000.
11. Weidenmann KA, Fleck C, Schulze V, et al. Mechanical properties of rope-reinforced aluminium extrusions under quasistatic loading conditions. *Int J Mater Res* 2007; 98: 39–46.
12. Martens A. *Handbuch der Materialkunde für den Maschinenbau*. Berlin: Springer, 1898.
13. Hammers T, Merzkirch M, Weidenmann KA, et al. Mechanisches Verhalten ausgewählter Werkstoffsysteme verbundstranggepresster Leichtbauprofile unter quasistatischer Belastung. In: *17. Symposium "Verbundwerkstoffe und Werkstoffverbunde," Bayreuth* 2009, pp.155–161.
14. Schoene C and Scala E. Multiple necking phenomena in metal composites. *Metallurgic Transact* 1970; 3: 3466–3469.
15. Vennett RM, Wolf SM and Levitt AP. Multiple necking of tungsten fibers in a brass-tungsten composite. *Metallurgic Transact* 1970; 1: 1569–1575.
16. Piehler HR. Plastic deformation and failure of silver-steel filamentary composites. *Trans TMS-AIME* 1965; 233: 12–16.
17. Shorshorov MK, Moguchii LN, Ustinov LM, et al. Investigation of the failure in tension of an aluminum alloy reinforced with steel wire. *Strength Mater* 1974; 7: 961–965.
18. Mileiko ST. The tensile strength and ductility of continuous fibre composites. *J Mater Sci* 1969; 4: 974–977.
19. Weidenmann KA, Fleck C, Schulze V, et al. Analysis of the microstructure and the residual stress state of aluminium extrusions reinforced with ropes. *Mat-wiss u Werkstofftech* 2005; 36: 307–312.
20. Chawla N, Andres C and Jones JW. Cyclic stress-strain behavior of particle reinforced metal matrix composites. *Scr Mater* 1998; 38: 1595–1600.
21. Corbin SF and Wilkinson DS. The influence of particle distribution on the mechanical response of a particulate metal matrix composite. *Acta Metall Mater* 1993; 42: 1311–1318.
22. Möck Ch. Residual stresses in continual, unidirectional reinforced fibre-composites and composite-constructions. *Z Werkstofftech* 1984; 15: 268–276.

23. Möck Ch. Residual stresses in continual, unidirectional reinforced fibre-composites and composite-constructions. *Z Werkstofftech* 1984; 15: 315–323.
24. Ashby MF. *Material selection in mechanical design*. 2nd ed. Butterworth Heinemann, 2004.
25. Merzkirch M, Weidenmann KA and Schulze V. Lifetime behaviour of unidirectionally wire reinforced lightweight metal matrix composites. *Int J Fatigue* 2013; 56: 60–68.

Appendix

Notation

A_0	Initial cross-sectional area
E_M	Young's modulus of the matrix
E_{RE}	Young's modulus of the reinforcing element
E_I	Young's modulus in region I of the composite
E_{II}	Young's modulus in region II of the composite
ΔL_F	Total length to fracture
L_0	Initial measuring length
L'_0	Adapted measuring length after failure of the reinforcing element
V_{RE}	Volume ratio of the reinforcing element
V_M	Volume ratio of the matrix
α	Parameter for the uniform elongation
β	Parameter for the necking elongation
ε_t	Total strain
ε_M	Total strain of the matrix
ε_M^F	Total strain to fracture of the matrix
ε_{RE}^F	Total strain to fracture of the reinforcing element
ε_{RE}^{*F}	Total strain to fracture of the reinforcing element within the composite
ε_C^{uni}	Uniform elongation of the composite
ε_M^{uni}	Uniform elongation of the matrix at $\sigma_{UTS,M}$
ε_{RE}^{uni}	Uniform elongation of the reinforcing element at $\sigma_{UTS,RE}$
σ_n	Nominal stress
σ_C	Stress within the composite
σ_M	Stress within the matrix
$\sigma_M(\varepsilon_{RE}^F)$	Stress within the matrix at total strain to fracture of the reinforcing element ε_{RE}^F
σ_{RE}	Stress within the reinforcing element
$\sigma_{y,M}$	Yield strength of the matrix
$\sigma_{y,RE}$	Yield strength of the reinforcing element
$\sigma_{UTS,M}$	Ultimate tensile strength of the matrix
$\sigma_{UTS,RE}$	Ultimate tensile strength of the reinforcing element
$\sigma_{UTS,C}$	Ultimate tensile strength of the composite
$\varepsilon_{t,cor}^{uni}$	Correction of the uniform strain
$\varepsilon_{t,cor}^{neck}$	Correction of the necking strain